PHYSICAL REVIEW C **66**, 021901(R) (2002)

Centrality and momentum-selected elliptic flow: Tighter constraints for the nuclear equation of state

P. Chung,[1] N. N. Ajitanand,[1] J. M. Alexander,[1] J. Ames,[1] M. Anderson,[5] D. Best,[2] F. P. Brady,[5] T. Case,[2] W. Caskey,[5] D. Cebra,[5] J. L. Chance,[5] B. Cole,[11] K. Crowe,[2] A. C. Das,[3] J. E. Draper,[5] M. L. Gilkes,[1] S. Gushue,[1,9] M. Heffner,[5] A. S. Hirsch,[7] E. L. Hjort,[7] W. Holzmann,[1] L. Huo,[13] M. Issah,[1] M. Justice,[4] M. Kaplan,[8] D. Keane,[4] J. C. Kintner,[12] J. Klay,[5] D. Krofcheck,[10] R. A. Lacey,[1] J. Lauret,[1] M. A. Lisa,[3] H. Liu,[4] Y. M. Liu,[13] J. Milan,[1] R. McGrath,[1] Z. Milosevich,[8] G. Odyniec,[2] D. L. Olson,[2] S. Panitkin,[4] N. T. Porile,[7] G. Rai,[2] H. G. Ritter,[2] J. L. Romero,[5] R. Scharenberg,[7] L. Schroeder,[2] B. Srivastava,[7] N. T. B Stone,[2] T. J. M. Symons,[2] J. Whitfield,[8] T. Wienold,[2] R. Witt,[4] L. Wood,[5] and W. N. Zhang[13]

(E895 Collaboration)

P. Danielewicz[6]

[1]*Departments of Chemistry and Physics, SUNY at Stony Brook, New York 11794-3400*

[2]*Lawrence Berkeley National Laboratory, Berkeley, California 94720*

[3]*Ohio State University, Columbus, Ohio 43210*

[4]*Kent State University, Kent, Ohio 44242*

[5]*University of California, Davis, California 95616*

[6] *Michigan State University, East Lansing Michigan 48824-1321 and Gesellschaft für Schwerionenforschung, Darmstadt D-64291, Germany*

[7]*Purdue University, West Lafayette, Indiana 47907-1396*

[8]*Carnegie Mellon University, Pittsburgh, Pennsylvania 15213*

[9]*Brookhaven National Laboratory, Upton, New York 11973*

[10]*University of Auckland, Auckland, New Zealand*

[11]*Columbia University, New York, New York 10027*

[12]*St. Mary's College, Moraga, California 94575*

[13]*Harbin Institute of Technology, Harbin 150001, People's Republic of China*

(Received 3 December 2001; published 20 August 2002)

Proton elliptic flow is studied as a function of impact parameter b, for two transverse momentum cuts in 2–6 A GeV Au+Au collisions. The elliptic flow shows an essentially linear dependence on b (for $1.5<b<8$ fm) with a negative slope at 2A GeV, a positive slope at 6A GeV, and near zero slope at 4A GeV. These selective flow measurements provide better understanding of the interplay of the different factors responsible for the generation of elliptic flow at AGS energies. In addition, extensive comparisons of the measured and calculated flow values indicate that such measurements offer much more stringent constraints for discriminating between various equations of state.

DOI: 10.1103/PhysRevC.66.021901 PACS number(s): 25.75.Ld

For several years now, the study of nuclear matter at high energy density has held the promise of providing valuable insights on the nuclear equation of state (EOS) and on the predicted phase transition to a quark-gluon plasma (QGP) [1–3]. At AGS energies of $\sim 1-14$ A GeV, elliptic flow has emerged as an invaluable probe of high density nuclear matter [4–8]. This flow has been attributed to a delicate balance between (i) the ability of compressional pressure to effect a rapid transverse expansion of nuclear matter and (ii) the passage time for removal of the shadowing of participant hadrons by the projectile and target spectators [6,9]. If the passage time is long compared to the expansion time, spectator nucleons serve to block the path of participant hadrons emitted toward the reaction plane, and nuclear matter is squeezed out perpendicular to this plane giving rise to negative elliptic flow. For shorter passage times, the blocking of participant matter is significantly reduced and preferential in-plane emission or positive elliptic flow is favored because the geometry of the participant region exposes a larger surface area in the direction of the reaction plane. Thus, elliptic flow is predicted to be negative for beam energies $\lesssim 4A$ GeV and positive for higher beam energies [4,6,10].

Recent theoretical studies of elliptic flow have suggested a sensitivity to the pressure at maximum compression [4,10,11] and thus to the stiffness of the EOS, and to possible QGP formation [6]. Despite this sensitivity, the commonly calculated patterns for elliptic flow very often do not constrain the EOS uniquely [6,7]. This being the case, it is important to investigate more specific elliptic flow observables which can give new and more detailed constraints for the EOS. In Ref. [8] we used elliptic flow measurements from 2–8 A GeV Au+Au reactions to probe the EOS. Recent calculations (discussed below) show that the study of differential flow $v_2(b)$ and $v_2(b,p_T)$ is much more powerful than the study of integral flow. Here we present much more selective measurements and show that they can resolve significant ambiguity in the nuclear compressibility. Furthermore, the pattern of quantitative results serves as evidence for a mechanistic understanding of the origin of elliptic flow [4,6,10].

TABLE I. Correction factors for reaction plane dispersion for several impact parameter ranges for the 2, 4, and 6 *A* GeV beam energies. Estimated systematic uncertainties are ~5%.

	Dispersion correction factor		
b range (fm)	2*A* GeV	4*A* GeV	6*A* GeV
$0<b<3$	1.71	2.64	4.65
$4<b<6$	1.22	1.59	2.47
$7<b<8$	1.26	1.99	2.86

The measurements were performed at the Alternating Gradient Synchrotron (AGS) at the Brookhaven National Laboratory. Beams of ^{197}Au at $E_{Beam}=2$, 4, and 6 *A* GeV [12] were used to bombard a ^{197}Au target of thickness chosen for a 3% interaction probability. Typical beam intensities resulted in ~10 spills/min with $\sim 10^3$ particles per spill. Charged reaction products were detected in the time projection chamber (TPC) [13] of the E895 experimental setup. The TPC located in the MPS magnet (typically at 1.0 Tesla) provided good acceptance and charge resolution for charged particles $-1<Z<6$ at all three beam energies [14]. However, a unique mass resolution for $Z=1$ particles was not achieved for all rigidities [19]. Data were taken in two experimental runs with a trigger which allowed for a wide range of impact parameter selections as presented below.

Our flow analysis follows the now standard procedure [15] of using the second Fourier coefficient, $v_2=\langle \cos 2\phi \rangle$, to measure the elliptic flow or anisotropy of the proton azimuthal distributions at midrapidity (normalized rapidity $|y_{\mathrm{c.m.}}|<0.1$). This distribution can be expanded as

$$\frac{dN}{d\phi} \propto [1+2v_1\cos(\phi)+2v_2\cos(2\phi)], \tag{1}$$

where ϕ represents the azimuthal angle of an emitted proton relative to the reaction plane. Near midrapidity in a symmetric system $v_1 \approx 0$. For each proton *i*, the reference azimuthal angle Φ_{plane} of the reaction plane is determined using [16] the vector $\mathbf{Q_i}=\Sigma_{j\neq i}^{n} w(y_j)\mathbf{p_T}_j/p_{Tj}$. Here, $\mathbf{p_T}_j$ and y_j represent, respectively, the transverse momentum and the rapidity of each baryon $j(Z\leqslant 2)$ in an event. The weight $w(y_j)$ is assigned the value $\langle p_x \rangle / \langle p_T \rangle$, where p_x is the transverse momentum in the reaction plane [9]. The average $\langle p_x \rangle$ is obtained from the previous pass of an iterative procedure employed for each energy and impact parameter selection.

The orientation of the impact parameter vector follows azimuthal symmetry about the beam axis. Therefore, the azimuthal distribution of the determined reaction plane should be uniform or flat. We have established that deviations from this uniformity can be attributed to deficiencies in the acceptance of the TPC and have applied rapidity and multiplicity dependent corrections following Ref. [8]. The corrections were applied for each of several impact parameter selections at each beam energy; they ensure the absence of spurious elliptic flow signals which might result from distortions in the reaction plane distribution. The dispersion of the reaction plane $\langle |\phi_{12}| \rangle /2$ was estimated for each impact parameter *b* via the subevent method [16]. These estimates for the reaction plane dispersion provide the dispersion corrections summarized in Table I; these corrections have been applied to the extracted flow values shown in Fig. 1 below.

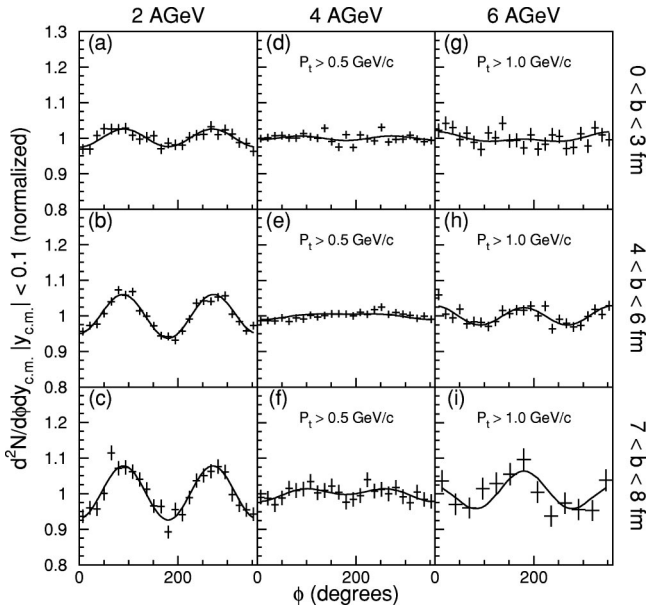

FIG. 1. Measured azimuthal distributions for Au+Au collisions. Distributions are shown for the impact parameter ranges of $0\leqslant b \leqslant 3$ fm, $4\leqslant b\leqslant 6$ fm and $7\leqslant b\leqslant 8$ fm and the beam energies of 2 (a), (b), (c), 4 (d), (e), (f), and 6 (g), (h), (i) *A* GeV, as indicated. The solid lines are drawn to guide the eye.

The event multiplicity of identified charged particles M_{filt} was used for centrality selection. That is, several multiplicity bins were selected in the range from 0.4 to 1.0 M_{max} where M_{max} is the point in the charged particle multiplicity distribution where the height of the distribution has fallen to half its plateau value [17]. Impact parameter estimates have also been made for these centrality selections, at each beam energy, via their respective fraction of the minimum bias cross section.

Figure 1 shows representative distributions in the azimuthal angle ϕ obtained at the energies of 2, 4, and 6 *A* GeV for midrapidity ($|y_{\mathrm{c.m.}}|<0.1$) protons. The panels from left to right represent the three beam energies, respectively, and from top to bottom the three impact parameter ranges of $0 \leqslant b \leqslant 3$, $4\leqslant b\leqslant 6$ and $7\leqslant b\leqslant 8$ fm. A p_T cut has been applied to the distributions shown for both the 4 and 6 *A* GeV data, as indicated. Within each *b*-range in Fig. 1, the previously reported transition from negative to positive elliptic flow at $\approx 4A$ GeV [8] is clearly seen. That is, the elliptic flow is negative at 2*A* GeV, positive at 6*A* GeV and essentially zero at 4*A* GeV. An apparent increase of the anisotropy of the distributions with increasing *b* can also be discerned for the 2 and 6 *A* GeV data shown in Fig. 1. We attribute this trend to an interplay of the changing geometry with the expansion of excited participant matter as discussed below.

Figure 2 shows the v_2 coefficients for the full p_T range, as a function of *b* for data (stars) obtained at 2, 4, and 6 *A* GeV in the three panels, respectively. These coefficients have been

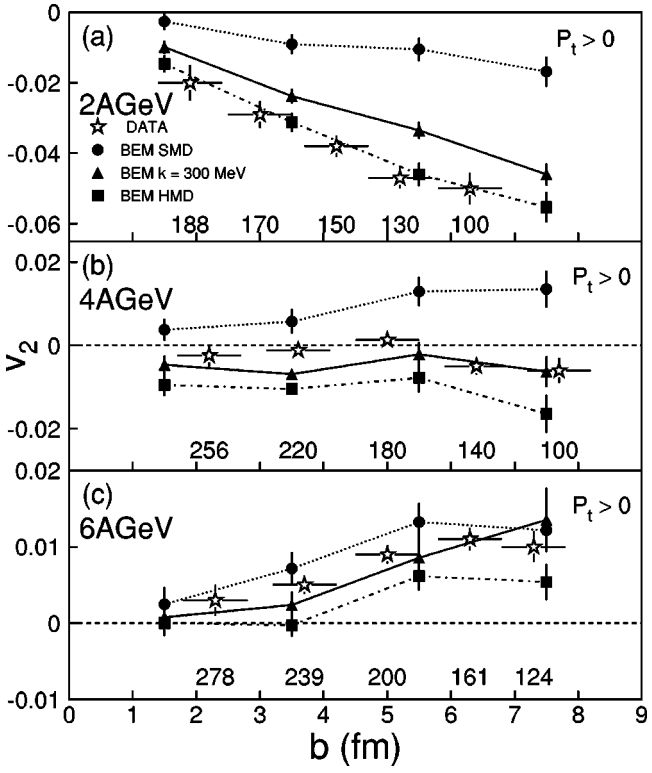

FIG. 2. v_2 as a function of b ($p_T>0$) for 2 (a), 4 (b), and 6 (c) A GeV Au+Au collisions. Experimental values are indicated by the open stars. The solid squares, circles, and triangles represent v_2 values from BEM calculations with a stiff ($K=380$ MeV), a soft ($K=210$ MeV), and an intermediate ($K=300$ MeV) momentum-dependent EOS, respectively. The average identified charged particle multiplicity M_{filt} is also indicated for each data point. The horizontal error bars indicate the estimated uncertainty for $\langle b\rangle$ for each bin. The error bars for the calculated values are statistical only; those for the data points include both the statistical and systematic errors. The solid, dotted, and dashed-dotted lines serve to guide the eye only.

obtained by evaluating the $\langle\cos 2\phi\rangle$ for each azimuthal distribution obtained for a given impact parameter at each beam energy. A correction has been applied to some of these coefficients to account for biases resulting from (i) low p_T acceptance losses in the TPC for the 2, 4, and 6 A GeV beams, (ii) high p_T acceptance losses in the TPC for the 2A GeV beam, and (iii) π^+ contamination of the proton sample at 4 and 6 AGeV [18,8]. A procedure for effecting these corrections has been detailed in Ref. [8]. That is, we first plotted the observed Fourier coefficient $\langle\cos 2\phi'\rangle$ vs p_T with p_T thresholds which allowed clean particle separation ($p_T\sim 1$ GeV/c). We then extracted the coefficients for the quadratic dependence of $\langle\cos 2\phi'\rangle$ on p_T. These quadratic fits are restricted by the requirement that $\langle\cos 2\phi'\rangle=0$ for $p_T=0$. Next, we corrected the proton p_T distributions for possible high and low p_T losses. A weighted average (relative number of protons in a p_T bin times the $\langle\cos 2\phi'\rangle$ for that bin) was then performed to obtain $\langle\cos 2\phi'\rangle$ for each beam energy. The corrections which result from this procedure are $\sim 5\%$ for the 4 and 6 A GeV beams and $\sim 15\%$ for the 2A GeV beam. Subsequent to these evaluations, the v_2 values were corrected for reaction plane dispersion using the procedures detailed in Refs. [8,15,16,19].

The v_2 values represented by the stars in Fig. 2 indicate an essentially linear dependence on impact parameter. The slope of this dependence is clearly negative and positive for the 2 and 6 A GeV data, respectively. By contrast, an essentially flat dependence is observed for the 4A GeV data suggesting that the beam energy at which the elliptic flow changes sign is not very sensitive to b for $0\lesssim b\lesssim 8$ fm. The approximately linear dependence exhibited by the data can be understood in terms of the collision geometry and the development of transverse expansion within the participant matter.

Consider first the situation for 2A GeV. The spectator velocities are relatively slow, and the passage time is relatively long. Expansion of the participant matter occurs rapidly while the spectators remain to shadow the in-plane directions, thus driving the escapees to squeeze-out perpendicular to the reaction plane. The expansion develops over a characteristic time of d/c_s while the spectators are present. Here, $c_s=\sqrt{\partial p/\partial e}$ represents the speed of sound for a given pressure p, and energy density e, and d is the perpendicular distance from the center of the participant region to the surface. The spectator passage time (estimated in sharp cutoff geometry) first increases and then remains essentially constant as b increases over the range of interest. On the other hand, the expansion time decreases with increasing b due to a decrease in d. It is this decrease in the expansion time coupled with an essentially constant passage time, which provides the driving force for more matter to escape the interaction region as b is increased, i.e., an increase in ''squeeze out'' with b. The magnitude of the ''squeeze out'' follows an approximately linear dependence because d is roughly proportional to $1/b$ for the Au+Au impact parameter range 1–8 fm.

At 6A GeV, the situation is reversed. The spectator passage time is very short compared to the expansion time and preferential in-plane emission dominates. In this case, the linear increase of v_2 with increasing impact parameter is driven by the initial spatial asymmetry of the nuclear overlap region or participant matter. This asymmetry is commonly characterized in terms of the width L_x and height L_y of the overlapping region via $\alpha_s=(L_y-L_x)/(L_y+L_x)$ [10] and can be shown to be nearly linearly proportional to the impact parameter for medium b values.

The essentially flat dependence of v_2 observed at 4A GeV suggests that, at the transition energy, the reduction in the expansion time (in competition with the spectator passage time) with increasing b, is compensated for by the (later) increased in-plane emission from the preserved initial spatial asymmetry.

The circles, squares, and triangles shown in Fig. 2, represent results from calculations with a recent version of the Boltzmann equation model BEM [6] which assumes a soft ($K=210$ MeV), a stiff ($K=380$ MeV), and an intermediate ($K=300$ MeV), EOS, respectively. The calculations include momentum dependent forces [20]. A comparison of the calculated v_2 values indicate sizable differences between the predictions for a stiff and a soft EOS for all three beam

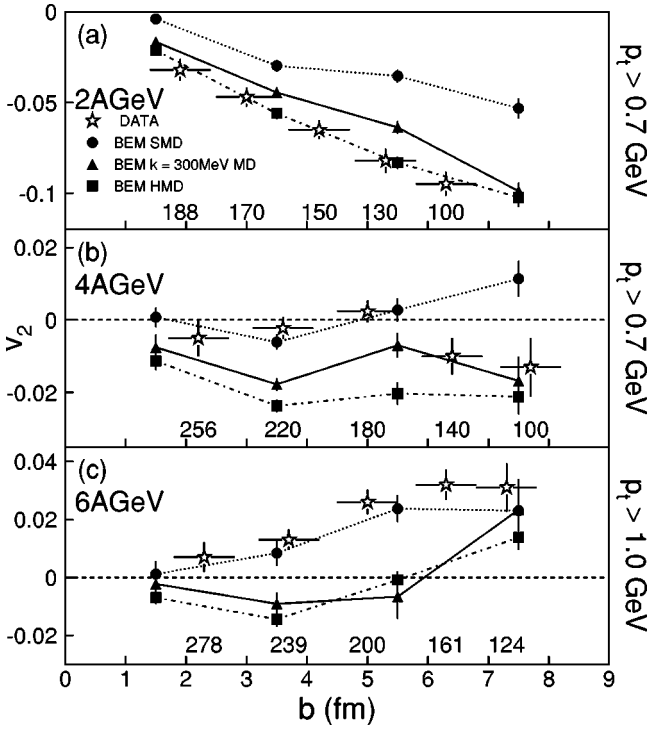

FIG. 3. Same as Fig. 2 except that a $p_T > 0.7$ GeV cut has been applied on the data and calculations at 2 and 4 A GeV and a $p_T > 1.0$ GeV cut has been applied at 6A GeV.

energies. For both 2 and 4 A GeV this distinction increases with increasing impact parameter indicating that the impact parameter dependence of elliptic flow gives an important constraint for the EOS. At 2A GeV, the v_2 values for the stiff EOS show good agreement, both in magnitude and trend, with the experimental data. At 4A GeV the measured v_2 values lie between the calculated result for a stiff and a soft EOS, and appear to be in better overall agreement with an intermediate form of the EOS. At 6A GeV the data are less compatible with a stiff EOS, but do not allow a clear distinction between the soft and the intermediate ($K = 300$ MeV) EOS. The latter result speaks to the need for additional cuts which might serve to remove such an ambiguity. Below, we investigate the effectiveness of applying transverse momentum cuts in conjunction with the impact parameter dependence.

Figure 3 compares experimental (stars) and calculated (circles, triangles, and squares) elliptic flow $v_2(b,p_T)$ for 2, 4, and 6 A GeV with p_t cuts as indicated. At each beam energy, the BEM calculations have been carried out for the same p_T and b selections applied to the data. Figure 3 indicates good agreement between the data and the calculated results for a stiff EOS at 2A GeV. At 4A GeV the data again show better overall agreement with the intermediate and soft EOS. At 6A GeV the comparison also indicates quite good agreement (both in magnitude and trend) between the data and the results from the calculations which assume a soft EOS. The latter agreement is in contrast to the results obtained from the comparison made in Fig. 2, and clearly indicates that the more selective flow $v_2(b,p_T)$, does indeed provide additional constraints for making a relatively clear distinction between the different EOS parameters at 6A GeV.

To summarize, we have studied proton elliptic flow selected by p_t and centrality in 2–6 A GeV Au+Au collisions. The elliptic flow shows an essentially linear dependence on b, in the range $1.5 \lesssim b \lesssim 8$ fm, with a negative slope at 2A GeV, an approximately zero slope at 4A GeV, and a positive slope at 6A GeV. These trends provide important mechanistic insights on the development and evolution of elliptic flow in relation to (a) the collision geometry, (b) the relative magnitude of the time for development of the transverse expansion, and (c) the passage time for removal of the shadowing of participant hadrons by the projectile and target spectators. Detailed comparison between the measured selective elliptic flow $v_2(b,p_t)$, and the results obtained from a relativistic Boltzmann-equation calculation, clearly shows that such elliptic flow measurements provide distinctly more stringent constraints for discriminating between different forms of the EOS. Such additional discriminating power is critical to the resolution of outstanding issues related to the stiffness of high density nuclear matter.

This work was supported in part by the U.S. Department of Energy under Grant Nos. DE-FG02-87ER40331.A008, DE-FG02-89ER40531, DE-FG02-88ER40408, DE-FG02-87ER40324, and Contract No. DE-AC03-76SF00098; by the U.S. National Science Foundation under Grant Nos. CHE-9871296, PHY-98-04672, PHY-9722653, PHY-0070818, PHY-9601271, and PHY-9225096; and by the University of Auckland Research Committee, NZ/USA Cooperative Science Program CSP 95/33.

[1] H. Stöcker and W. Greiner, Phys. Rep. **137**, 277 (1986).
[2] *Quark Matter '96, Procedings of the 12th International Conference on Ultra-Relativistic Nucleus-Nucleus Collisions, Heidelberg, Germany*, 1996, edited by P. Braun-Munzinger *et al.* [Nucl. Phys. **A610**, 1c (1996)].
[3] W. Reisdorf and H.G. Ritter, Annu. Rev. Nucl. Part. Sci. **47**, 663 (1997).
[4] H. Sorge, Phys. Rev. Lett. **78**, 2309 (1997).
[5] J. Barrette *et al.*, Phys. Rev. C **56**, 3254 (1997).
[6] P. Danielewicz *et al.*, Phys. Rev. Lett. **81**, 2438 (1998).
[7] Bao-An Li *et al.*, Phys. Rev. C **60**, 011901(R) (1999).
[8] C. Pinkenburg *et al.*, Phys. Rev. Lett. **83**, 1295 (1999).
[9] P. Danielewicz, Phys. Rev. C **51**, 716 (1995).
[10] J.-Y. Ollitrault, Phys. Rev. D **46**, 229 (1992).
[11] J.-Y. Ollitrault, Phys. Rev. D **48**, 1132 (1993).
[12] Actual beam energies are 1.85, 3.9, and 5.9 A GeV, respectively.
[13] G. Rai, IEEE Trans. Nucl. Sci. **37**, 56 (1990).
[14] G. Bauer, Nucl. Instrum. Methods Phys. Res. A **386**, 249 (1997).

[15] M. Demoulins *et al.*, Phys. Lett. B **241**, 476 (1990); M. Demoulins, Ph.D. thesis, University Paris Sud, 1989, Report No. CEA-N-2628, CEN Saclay, 1990.
[16] P. Danielewicz and G. Odyniec, Phys. Lett. **157B**, 146 (1985).
[17] H.H. Gutbrod, Rep. Prog. Phys. **52**, 1267 (1989).
[18] Unique separation of π^+ and protons was not achieved for all rigidities at all beam energies.
[19] J.-Y. Ollitrault, nucl-ex/9711003.
[20] P. Danielewicz, Nucl. Phys. **A673**, 375 (2000).